In Situ Scanning Tunneling Microscopy of a Redox Molecule as a Vibrationally Coherent Electronic Three-Level Process

Esben P. Friis,[‡] Yurij I. Kharkats,[§] Aleksander M. Kuznetsov,[§] and Jens Ulstrup*[,‡]

Department of Chemistry, Technical University of Denmark, DK-2800 Lyngby, Denmark, and The A. N. Frumkin Institute of Electrochemistry of the Russian Academy of Sciences, Leninskij Prospect 31, 117071 Moscow, Russia

Received: April 3, 1998; In Final Form: June 12, 1998

We provide a theoretical frame for in situ scanning tunneling microscopy (STM) of adsorbate molecules with low-lying redox levels strongly coupled to the environmental nuclear motion. The STM process is viewed as a coherent two-step electron transfer (ET) involving electron exchange between the local redox level and the manifolds of electronic levels in the substrate and tip. The notion coherence is here taken to imply that the intermediate electron or hole state after the first ET step does not fully relax vibrationally before the second ET step. These views and the theoretical formalism are appropriate to in situ STM of large transition metal complexes and redox metalloproteins. The formalism offers two kinds of spectroscopic features. One is the relation between the tunnel current and the bias voltage at fixed overvoltage of either the tip or the substrate relative to a reference electrode. The other one is the tunnel current dependence on the overvoltage, at fixed bias voltage. Recent data on tunneling current patterns for adsorbed or covalently tethered metalloporphyrins and the blue single-copper protein azurin are discussed in terms of the formalism.

1. Introduction

Electron tunneling patterns of redox metalloproteins have been characterized in considerable detail.[1−16] These structurally organized large molecules have recently come to offer new probes for single-molecule electronic conduction in in situ scanning tunneling (STM),[17−23] offering particularly the following new perspectives.

(1) In situ STM monitors the molecules in their natural, *aqueous* functional medium. This raises, however, a number of recognized issues such as independent substrate surface and tip potential control, adsorbate immobilization, etc.[24,25]

(2) The metal centers represent low-lying HOMO and LUMO levels well separated from environmental electronic states but strongly coupled to the vibrational nuclear environment.[26−30] In this way in situ STM offers insight into molecular conduction imaging, and a new case for otherwise elusive long-range, vibrationally or conformationally *coherent* three-level electron transfer (ET) process.[30]

(3) In situ STM holds the perspective of spectroscopy-like imaging of electronic function, rooted in the *independent* control of the electrochemical potentials of the substrate and tip toward a common reference electrode. The tunnel current can therefore be controlled *either* by the bias potential for a given electrochemical potential of one of the electrodes relative to the reference electrode, or by the variation of the overpotential of *both* electrodes, at fixed bias voltage.[21]

In this work we address these tunnel spectroscopic features theoretically. The in situ STM process is first viewed as a three-level electronic-vibrational/conformational process in the sense noted.[28,29] We focus particularly on *two* issues of importance to in situ STM of large molecules of the kind noted. One is the view of the two-step ET process as a vibrationally or conformationally *coherent* two-step ET process. This notion is detailed below. The formalism of this feature rests on the theory of vibrationally coherent transitions in other chemical thermal and optical processes.[31] The other focus is on the *nuclear* coupling, most conspicuously reflected in the solvent reorganization Gibbs free energy. This quantity is conceptually and formally well understood for ET processes in homogeneous or semi-infinite homogeneous systems.[32] The solvent reorganization Gibbs free energy, however, takes different forms and numerical values in the doubly heterogeneous ET system consisting of the planar substrate−solution interface, the finite-size molecular redox center, and the metallic tip. Such an analysis holds new insight into the observable tunnel current/bias voltage and -/overvoltage relations based on these two features and has not been undertaken before. The correlations are supported by recent experimental data for metalloporphyrins adsorbed on highly oriented pyrolytic graphite (HOPG)[21,22] and for the blue copper protein azurin chemisorbed on Au(111) surfaces.[23,33]

Electron tunneling through a low-lying redox level in the in situ STM configuration is shown schematically in Figure 1. The substrate and tip electrodes are represented as two electronic continua. Both electrodes are viewed as planar, but finite-size tip effects on the nuclear relaxation will be considered in Section 5. Much of the discussion below can also be extended to discrete electronic structural effects caused by the tip shape.[28] The vacant redox level in the oxidized adsorbate is represented by a conspicuous indentation in a barrier constituted by the LUMO of the aqueous or protein medium. This feature enhances tunneling, but the redox level is also strongly coupled to the nuclear environment, and low enough that *fluctuations* in the nuclear configuration can take the level close to the populated electronic levels, ϵ_R, near the Fermi level of the

* Corresponding author: telephone, +45 45252359; fax: +45 45883136; e-mail, JU@Kemi.DTU.DK.
‡ Technical University of Denmark.
§ A. N. Frumkin Institute of Electrochemistry.

S1089-5639(98)01732-0 CCC: $15.00
Published on Web 09/12/1998

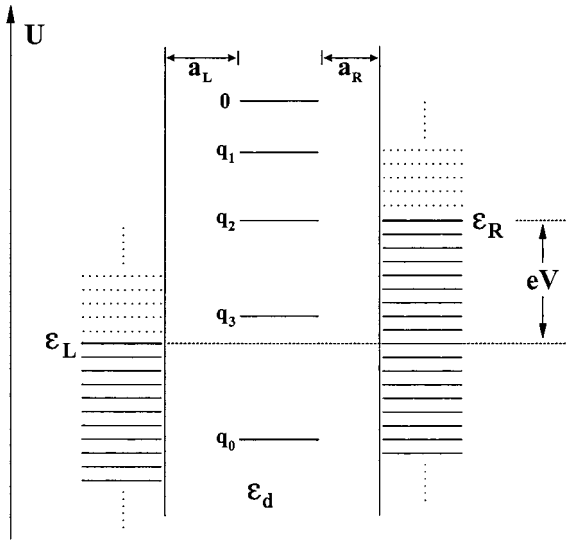

Figure 1. Energy diagram of in situ three-level electronic-vibrational STM. Electronic energy manifolds of the positively (ϵ_L, left) and negatively (ϵ_R, right) biased electrode are coupled via the (initially vacant) molecular redox level in the tunnel gap. Fluctuations in the nuclear coordinate(s) q lower the level to values near the Fermi level ϵ_{RF} where ET predominantly occurs. Continued relaxation takes the filled molecular level to lower values where ET to the positively biased electrode occurs prior to full vibrational relaxation.

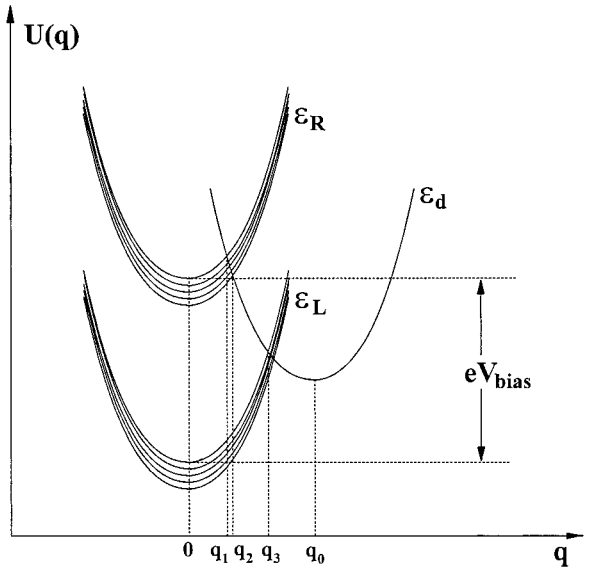

Figure 2. Nuclear potential (Gibbs free) energy surfaces corresponding to the electronic levels in Figure 1.

negatively biased electrode, ϵ_{RF} ("right"). After this step at least three further scenarios can be envisaged.[30]

(i) The electron can proceed directly to vacant levels in the positively biased electrode, ϵ_L, in a three-level resonance mode. This is analyzed elsewhere.[26,27]

(ii) The temporarily filled (reduced) redox level can proceed to full vibrational or conformational relaxation well below both Fermi levels ϵ_{LF} and ϵ_{RF}. The second ET step, from the reduced molecule to vacant levels in the positively biased electrode, then requires renewed thermal activation. This mode is little different from two *sequential*, i.e., fully equilibrated *electrochemical* single-ET steps involving an orientationally fixed depolarizer molecule. This mode has also been analyzed previously.[28]

(iii) In the third ET mode the reduced adsorbate level *begins* to relax vibrationally, i.e., to move downward in the scheme of Figure 1. However, before full relaxation is reached, and the level has passed the Fermi level of the positively biased ("left") electrode, the second ET occurs. This mode can be called vibrationally or conformationally coherent two-step ET because non-Markovian features and electronic features of *both* transitions now appear explicitly in the tunnel current. The three-level potential surface configuration shown in Figure 2 is complementary to Figure 1. The nuclear equilibrium is *displaced* on the first ET but restored after the second step, apart from the vertical displacement caused by the bias voltage V_{bias}, i.e., by eV_{bias} (> 0) where e is the electronic charge. Similar considerations apply to two-step processes where the local redox level is initially filled (reduced) and well below both Fermi levels. Such patterns in homogeneous solution were addressed early[34−37] and have come in recent intense focus in the new areas of ultrafast (subpico- and femtosecond) ET processes in chemistry and biology.[38−42]

In this report we address explicitly the coherent two-step mode of the in situ STM/redox adsorbate system. Particularly we show that this mode provides interesting structures in the relations between the observed tunnel current, i_{coh}, and *two* voltage quantities, i.e., the bias voltage and the overvoltage, η; cf. above. These relations are different from similar correlations in both electrochemical single-ET processes and from sequential, i.e., equilibrated two-step electrochemical processes. They hold, therefore, prospects for the otherwise elusive distinction between these two mechanisms.

2. Current−Voltage Relations for Coherent Three-Level ET in the in Situ STM/Redox

Adsorbate Configuration. The coherent two-step in situ STM tunnel current in the configurations in Figures 1 and 2 is controlled by the bias voltage, the overvoltage of, say, the negatively biased electrode, the total molecular, solvent, and protein reorganization Gibbs free energy, and the electronic tunnel factors. The latter couple electronically the redox level with electronic levels in the substrate and tip, through the intermediate solvent or protein "matter".

We consider first separately the two-step ET process represented by Figures 1 and 2. Subsequent relation to observed tunnel current/voltage relations will require parallel incorporation of *both* ET and the "hole transfer" mode where the ET step order is inverted. Using the theory of coherent diabatic two-step ET processes,[31,36,37] the following tunnel current form for ET through the *vacant* local redox level can be derived:

$$t^{e}_{coh}(\eta;V_{bias}) = \frac{\pi e}{E_R\hbar^2[k_BT|U^*_{R,mol} - U^*_{L,mol}|]^{1/2}} \times \int_{-\infty}^{\infty} d\epsilon_R f(\epsilon_R)\rho(\epsilon_R)[T_{R,mol}(\epsilon_R;\eta;V_{bias})]^2 \exp\left\{-\frac{[E_R - e\eta - \alpha eV_{bias} - (\epsilon_R - \epsilon_{RF})]^2}{4E_Rk_BT}\right\} \times \int_{-\infty}^{\epsilon_R} d\epsilon_L[1 - f(\epsilon_L + eV_{bias})]\rho(\epsilon_L)[T_{L,mol}(\epsilon_L;\eta;V_{bias})]^2 \quad (1)$$

This form is quite transparent as noted by the following observations.

(1) The Fermi functions, $f(\epsilon_R)$ and $f(\epsilon_L)$ represent the metallic level populations in the negatively ("right") and positively ("left") biased electrode, respectively

$$f(\epsilon_S) = \frac{1}{1 + \exp[(\epsilon_S - \epsilon_{SF})/k_BT]} \qquad S = R, L \quad (2)$$

where k_B is Boltzmann's constant and T the temperature. All energies are counted from the Fermi energy of the negatively biased electrode. $\rho(\epsilon_R)$ and $\rho(\epsilon_L)$ are the corresponding electronic level densities.

(2) The transition from the negatively biased electrode to the local level is associated with the activation Gibbs free energy where E_R is the total reorganization Gibbs free energy, and η the overvoltage of the negatively biased electrode relative to a reference electrode. α ($0 < \alpha < 1$) is the fraction of the bias potential drop ($V_{bias} > 0$) at the site of the redox level. E_R is considered separately in Section 3.

(3) $T_{R,mol}(\epsilon_R;\eta;V_{bias})$ and $T_{L,mol}(\epsilon_L;\eta;V_{bias})$ are the electron-exchange factors for ET between the local center, and given metallic levels in the negatively and positively biased electrode, respectively. $T_{R,mol}$ and $T_{L,mol}$ can be represented by the individual metallic and molecular wave functions, or by density functional methods.[43] Here we shall use cruder but operationally adequate tunnel factors of the specific form

$$[T_{R,mol}(\epsilon_R;\eta;V_{bias})]^2 \approx [T^0_{R,mol}]^2 \exp\left\{-\frac{2}{\hbar}\sqrt{2m_e[U^0_R + e\eta + \alpha eV_{bias} - (\epsilon_R - \epsilon_{RF})]}\alpha_R\right\}$$

$$[T_{L,mol}(\epsilon_L;\eta;V_{bias})]^2 \approx [T^0_{L,mol}]^2 \exp\left\{-\frac{2}{\hbar}\sqrt{2m_e[U^0_R + e\eta + (1-\alpha)eV_{bias} - (\epsilon_L - \epsilon_{LF})]}\alpha_L\right\} \quad (3)$$

where m_e is the electronic mass, U^0_R the barrier height for the transition from the negatively biased electrode to the adsorbate at equilibrium ($\eta = V_{bias} = 0$), and $2\pi\hbar$ Planck's constant. $T^0_{R,mol}$ and $T^0_{L,mol}$ are energy quantities independent of η, V_{bias}, ϵ_R and ϵ_L. a_R and a_L are, finally, the spatial extensions of the tunnel gaps (Figure 1).

(4) The pre-integral factor reflects the intermediate state relaxation process and depends weakly on the energy quantities. $U^*_{R,mol}$ is, more specifically the (Gibbs free) energy at the crossing of the reactant and intermediate state potential surfaces at electronic energies around the Fermi energy. $U^*_{L,mol}$ is similarly, the energy at the intermediate and product state potential surface crossing at $\epsilon_L \cong \epsilon_{LF}$.

Equations 1 and 2 represent the correlations between the coherent tunnel current and either the bias voltage or the overvoltage, for the ET mechanism involving temporary population solely of the initially *vacant* redox level. The equations apply to real systems as long as the fluctuationally induced vacant level positions set out from a position *above* the Fermi level of the positively biased electrode, i.e., at overvoltages $|e\eta| \leq E_R - eV_{bias}$. A merit of this in situ STM configuration is that large overvoltages, $|e\eta| > E_R - eV_{bias}$ can be probed such as shown recently for adsorbed and covalently linked metalloporphyrins.[21,22] Such overvoltages would place the level initially *below* both Fermi levels. The in situ STM mode here sets out from the fully relaxed, reduced adsorbate level, and the order of the two ET steps would be reversed in a "hole transfer" mode.

Full incorporation of these features can be achieved by a single scheme of master equations. We provide details of such a scheme elsewhere[44] and presently approach the combined electron and hole transfer in a pragmatic way, by adding the hole transfer current term, i^h_{coh}, in a form analogous to eq 1. i^h_{coh} is thus

$$i^h_{coh}(\eta;V_{bias}) = \frac{\pi e}{E_R\hbar^2[k_BT|U^*_{R,mol} - U^*_{L,mol}|]^{1/2}} \times \int_{-\infty}^{\infty} d\epsilon_L[1 - f(\epsilon_L + eV_{bias})]\rho(\epsilon_L)[T_{L,mol}(\epsilon_L;\eta;V_{bias})]^2 \exp\left\{-\frac{[E_R + e\eta - (1-\alpha)eV_{bias} + (\epsilon_L - \epsilon_{LF})]^2}{4E_Rk_BT}\right\} \times \int_{\epsilon_L}^{\infty} d\epsilon_R f(\epsilon_R)\rho(\epsilon_R)[T_{R,mol}(\epsilon_R;\eta;V_{bias})]^2 \quad (4)$$

where all the symbols were defined above. The *overvoltage* still refers to the *cathodic* overvoltage of the negatively biased electrode. As η increases, the filled level is therefore lowered further, *increasing* the activation Gibbs free energy for ET from the filled redox level to the positively biased electrode. This step is the thermally activated first step in the hole transfer channel, and $e\eta$ (<0) therefore appears in eq 4 with a *positive* sign.

The observed current in the coherent two-step tunnel mechanism is, then

$$i_{coh} = i^e_{coh} + i^h_{coh} \quad (5)$$

Together with eqs 1−4 this is the form to be compared with experimental data. i^e_{coh}, however, dominates entirely at overpotentials $|e\eta| \leq E_R - eV_{bias}$, while i^h_{coh} dominates when $|e\eta| \geq E_R - eV_{bias}$. Equations 1−5 will be analyzed numerically in Section 4, but first we attend to the important quantity E_R which takes particular forms in the gap regions between the infinitely planar metallic substrate and the finite-size metallic tip region.

3. Solvent Reorganization Gibbs Free Energy in the in Situ Adsorbate STM

Configuration. The solvent reorganization Gibbs free energy has long been recognized as a most central quantity in ET processes in homogeneous solution,[45,46] and in electrochemical[47−52] and biological processes.[53] Simple forms are available for a variety of *models*,[32] where representation of the reactant molecules is as conducting spheres in a structureless isotropic uniform dielectric medium.[45] Other models, appropriate to redox metalloproteins, rest on views of the protein as a dielectric globule of low dielectric constant enclosing a spherical conducting metallic center, and embedded in a dielectric medium of larger dielectric constant.[54,55]

The model shown in Figure 3 is appropriate to the in situ STM configuration of a redox transition metal complex. The molecular adsorbate is represented as a conducting sphere of radius a, centered at a distance d ($\cong a$) from an infinite conducting substrate surface. The tip is represented as an approximately spherical conducting region with radius R close to the molecule. The molecular and tip centers are aligned perpendicularly to the surface. This configuration is by far the most tractable, and dominates the tunnel process because it gives both the most favorable (highest) tunnel factor and the most favorable (smallest) reorganization Gibbs free energy. The gap region is filled with a uniform, isotropic structureless dielectric with the optical and static dielectric constants ϵ_o and ϵ_s, respectively. This configuration is clearly different from electrochemical ET reorganization and has not been considered before. A particular observation is that, since electron localization is only on the molecule, the reorganization Gibbs free energy must be the same for ET between the molecule and *either* of the two electrodes.

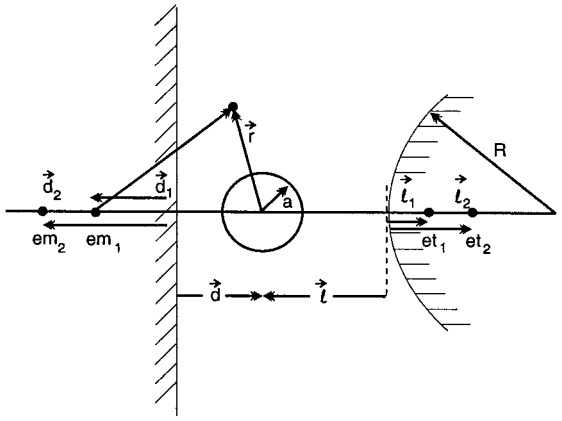

Figure 3. A simple model for in situ STM of a spherical molecular adsorbate in a structureless continuous dielectric medium between a planar substrate (left) and a (locally) spherical tip (right). Distances and image charges are indicated. The calculation of the solvent reorganization Gibbs free energy described in the text corresponds to this configuration.

The solvent reorganization Gibbs free energy of the model in Figure 3 is

$$E_R = (\epsilon_o^{-1} - \epsilon_s^{-1})\left\{\frac{e^2}{2a} + \sum_{n=1}^{\infty}\left[\frac{e(em_n)}{2(d+d_n)} + \frac{e(et_n)}{2(l+l_n)}\right]\right\} \quad (6)$$

em_n and et_n are fictitious image charges in the substrate metal and tip, respectively. em_n is located at the distance d_n from the substrate−solution interface inside the metal, and along the normal from the molecular center. et_n is located similarly inside the tip. The image charges and their locations are given by the recurrency relations, eqs A14−A18 in the Appendix. E_R thus depends on the space parameters a, d ($\geq a$), l, and R ($\geq l + d$). The first term in eq 6 represents an "isolated" molecule. All other terms originate from the metal and tip and have essentially a 2-fold effect. One is a more restrictive limit of the dielectric volume, leading to smaller E_R than for a semi-infinite medium. The other one is a different electric field distribution compared to infinite or semi-infinite solvation configurations.

An interesting limiting case emerges when the tip radius is large and the tip approaches a second planar interface. This is a useful heuristic aid but cannot represent physical reality as molecular resolution of in situ STM would then be lost. The following simple E_R form can be derived in this limit by a procedure similar to the one above

$$E_R = (\epsilon_o^{-1} - \epsilon_s^{-1})\left(\frac{e^2}{2a} - \frac{e^2}{4h}\right)\sum_{n=1}^{\infty}\frac{1}{n(n-{}^1/_2)} \quad (7)$$

where h is now the gap between the two planar electrodes. The first term in this series is the reorganization Gibbs free energy on ET between an infinite planar interface and an adjacent spherical molecule. The second term holds the corrections from all the image terms and vanishes as the tip−substrate gap approaches large values. These terms are always *negative* and reduce E_R due to the reduced space of repolarizable solvent.

4. Numerical Investigations of in Situ STM Current−Voltage Relations and the Solvent

In this Section we illustrate numerically the analytical results of Sections 2 and 3. We address first the tunnel current, and then the solvent reorganization Gibbs free energy.

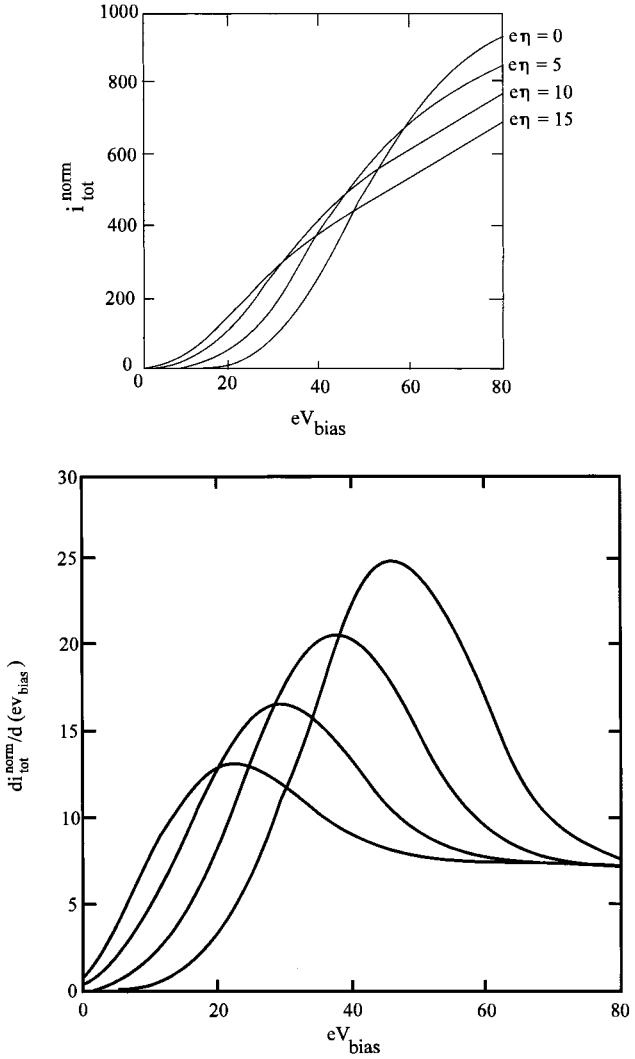

Figure 4. (a, top) Current/bias voltage relations for the in situ STM configuration in Figures 1 and 2 calculated from eqs 1−5. The correlations show specifically the variation of the double integrals in eqs 1−5, i.e., $i_{tot}^{norm} \propto i_{coh}^{e} + i_{coh}^{h}$, cf. eq 5. The pre-integral factors, the level densities $\rho(\epsilon_L)$ and $\rho(\epsilon_R)$, and the approximately constant tunnel factors are disregarded. Energy quantities are in units of k_BT (=25 mV). $E_R = 20$; $\alpha = 0.5$. The four curves correspond to different overvoltages, $e\eta$, indicated to the right. The noticeable inflection points follow the variation of $e\eta$. (b, bottom) Derivatives of the correlations in (a), showing more clearly the structural feature as $e\eta$ crosses the Fermi level of the negatively biased electrode.

4.1. Tunnel Current/Bias Voltage and Tunnel/Overvoltage Relations. Suitable parameter values are $E_R = 0.25-0.5$ eV and $\alpha = 0.5$. The bias voltage is brought to vary from zero to E_R while the overvoltage range is wide enough to take the redox level from its initial position above (below) the Fermi level of the negatively (positively) biased electrode to values well on the other side of the appropriate Fermi levels.

Figure 4a shows the current/bias voltage relation at different, fixed overvoltages. The current rises weakly, i.e., more slowly than exponentially with increasing bias voltage over ranges which exceed significantly $E_R - e\eta$. The most distinctive feature is an inflection point at a bias voltage which follows $2(E_R - e\eta)$. This point reflects the molecular level crossing of the Fermi level of the negatively biased electrode. This is seen more clearly in Figure 4b which shows the derivative of the current/bias voltage relation which is approximately Gaussian in the representation of eqs 1−5.

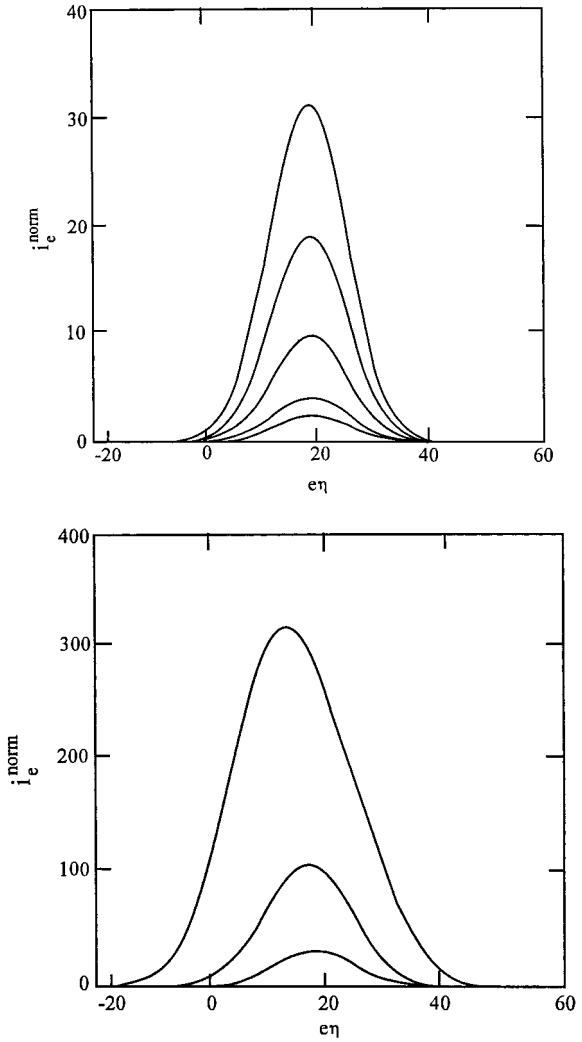

Figure 5. (a, top) Variation of the in situ electron-transfer STM current, i_{coh}^{e}, normalized as in Figure 4, with the overvoltage at different bias voltages. Energy quantities in units of k_BT (=25 mV). $E_R = 0.5$ eV, $\alpha = 0.5$. Increasing currents correspond to the bias voltages 25, 50, 100, 150, and 200 mV. The maximum is at $e\eta \approx E_R$ at small bias voltage. At large bias voltage the maximum is shifted to smaller values and the correlations are increasingly asymmetric. (b, bottom) Same as (a), except that the increasing currents correspond to the bias voltages 200, 400, and 800 mV.

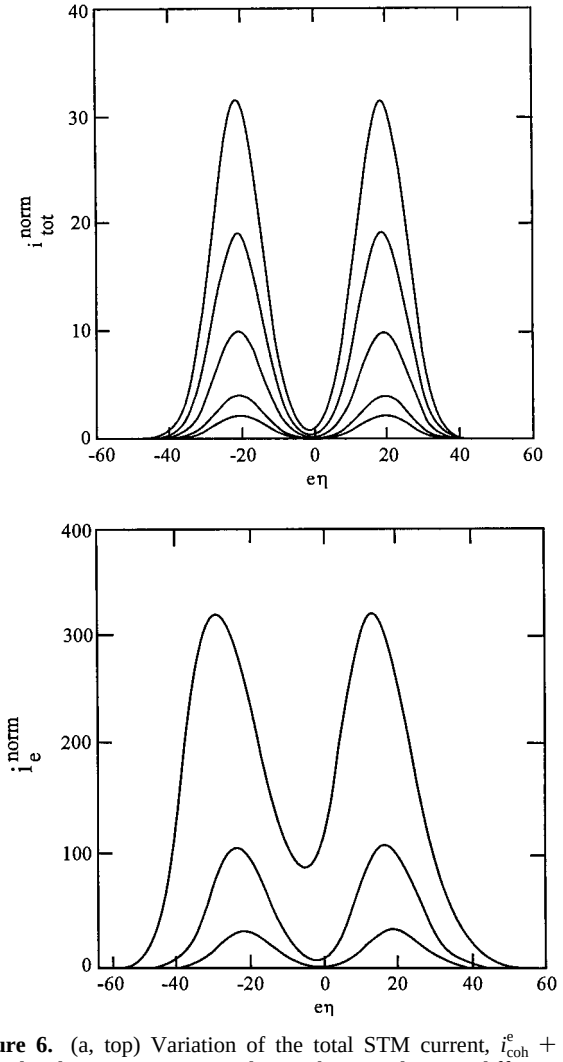

Figure 6. (a, top) Variation of the total STM current, $i_{coh}^{e} + i_{coh}^{h}$, normalized as in Figures 4 and 5, with overvoltage at different bias voltages. Same parameters and order as in Figure 5a. The strongly peaked feature to the right is dominated by *electron* transfer, the one to the left by *hole* transfer. (b, bottom) Similar correlation with the same parameters as in Figure 5b.

Figure 5 shows the *electron transfer* current/overvoltage relations at different bias voltages. The initial level position is above the Fermi level of the negatively biased electrode. There is a strong maximum approximately at $|e\eta| \approx E_R$. As the bias voltage increases, the maximum is shifted slightly to smaller values and the asymmetry of the correlation increases. The halfwidth is a convolution of E_R with eV_{bias} and begins to increase notably above E_R at $eV_{bias} > 0.25$ eV. An analogous relation in the range of positive $e\eta$ is obtained for hole transfer.

Figure 6 shows the sum of the electron and hole components for the same parameters as in Figure 5. In a given positive or negative overvoltage range, the current is first entirely dominated by *either* electron *or* hole transfer with maxima at $|e\eta| \approx E_R + \alpha eV_{bias}$. The absolute values of the current increase with increasing V_{bias} and the shape of the electron and hole current components become strongly asymmetric, with a slower falloff toward positive $e\eta$.

An overall observation is thus that the observed current/overvoltage relation is expected to show a maximum for small bias voltages, located at negative $e\eta$ for electron and at positive $e\eta$ for hole transfer. At large bias voltage, electron and hole transfer contribute comparably over larger overvoltage ranges, and resolution of the two components in a given range of negative or positive $e\eta$ can even be expected.

4.2. Solvent Reorganization Gibbs Free Energy. The two most interesting determining parameters for E_R are the tip radius R and the tip−substrate gap h. The most appropriate case is, moreover, when the molecular sphere is at contact distance with the substrate, i.e., $d = a$. Figure 7 shows the dependence of E_R on the gap width $l = h - d$. E_R approaches the value for a metallic sphere at large distances, but drops to about 60% of this value when the tip approaches the molecular sphere. Since the tunnel current depends exponentially on E_R, this result is interesting because it shows that short tunnel distances are approximately equally favored by the *electronic* tunnel factor and the *nuclear* activation Gibbs free energy factor. The physical origin of the latter is that the volume of solvent inertial repolarization is increasingly confined as the tip is taken closer to the molecular adsorbate. Figure 8 shows, finally, the dependence of E_R on the tip radius. E_R decreases by up to one-third as R increases from notably smaller values than the

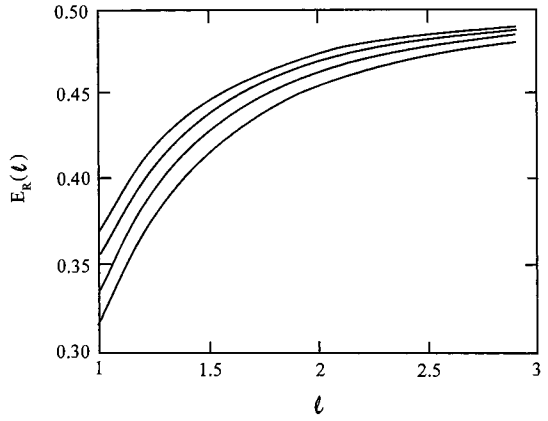

Figure 7. Dependence of $E_R(a/e^2)$ on the gap distance $l = h - d$ for different tip radii (Figure 3). The spherical molecule is in contact with the substrate ($d = a$). Distances in units of the molecular radius a. $E_R(a/e^2) \rightarrow 0.5$ in the absence of the tip. This value is represented by the first term on the right-hand side of eq A21, i.e., $E_R(l \rightarrow \infty) = (e^2/a)(\epsilon_o^{-1} - \epsilon_s^{-1})$. The different curves correspond to different tip radii, i.e., from top to bottom $R/a = 1$, 1.5, 3, and 10.

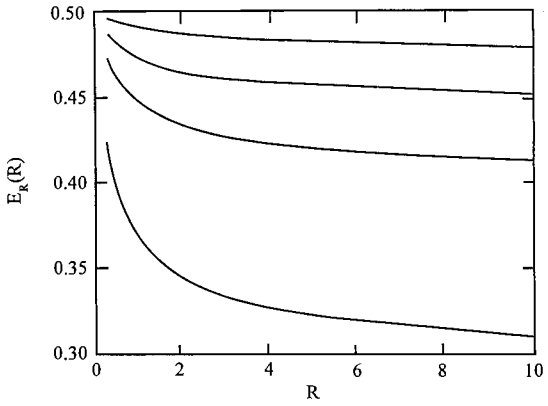

Figure 8. Dependence of $E_R(a/e^2)$ on the tip radius at different gap widths. Normalized distances and E_R as in Figure 7. The different curves represent, from top to bottom the following values of l/a: 1, 1.5, 2, and 3.

molecular adsorbate radius (corresponding to atomic tip dimensions) to notably larger values. This is again associated with the volume of repolarized solvent

5. Some Data in Support of Coherent, Vibrationally Induced Two-Step ET Mechanisms of in Situ STM of Transition Metal Complex and Redox Metalloprotein Adsorbates

Data which directly support the current−voltage patterns above are scarce. This is because such data require high adsorbate stability at the molecular level and because of constraints on the physical and chemical properties of the adsorbates as probe systems in the coherent, two-step ET mode. We consider three recent in situ STM systems which exhibit important features in keeping with expectations from the theoretical frame above.

5.1. In Situ Current−Voltage Relations of Fe−Protoporphyrin IX Adsorbed on Highly Oriented Pyrolytic Graphite (HOPG). Tao investigated the in situ STM current−overvoltage relations of protoporphyrin IX adsorbed on HOPG.[21] The apparent height at constant tunnel current (30 pA) and bias voltage (0.1 V) passed through a maximum close to the reduction potential. The maximum height is about five times higher than at potentials 0.2−0.3 V on either side. No such effect was found for the metal-free ligand which has no accessible redox levels. The halfwidth was ≈0.2 eV. This would correspond to $E_R \approx 0.55$ eV if convolution with the bias voltage is disregarded. Convolution means that the actual E_R is smaller, i.e., $E_R \approx 0.3-0.4$ eV, and not far from values calculated by the simple model in Section 3. Smaller theoretical values would emerge if nonlocal dielectric features or other solvent structural effects were introduced.

The maximum and the magnitude of the current variation are in line with the notion of coherent two-step ET. A discrepancy is that the maximum appears around the reduction potential E^0 rather than at $E^0 - E_R + |eV_{bias}| \approx E^0 - 0.2$ V. The potential distribution in the gap region could lower the discrepancy by ≈50 mV, but the origin of the remaining difference so far eludes identification. This feature seems to be apparent also in the two systems addressed below.

5.2. Current/Bias Voltage Relations of Covalently Immobilized Metalloporphyrins on Gold(111). In a recent report Tao, Lindsay, and their associates recorded current/bias voltage relations of several redox metalloporphyrin complexes, covalently tethered to a gold(111) surface in contact with an electrochemically inert solvent (mesitylene).[22] Electron tunneling here is via temporary population of the intermediate redox level. The data are paralleled by related observations of inelastic tunneling through phthalocyanines in metal−insulator−adsorbate−metal configurations.[61,62] The observed derivative current/bias voltage follows broadly the Gaussian dependence expected on the basis of the formalism in eqs 1−5, but there are two notes of observation. One is that, as for the data of Tao, the Gaussian derivative form is *also* formally in keeping with other tunneling mechanisms, resonance tunneling in particular. The other one is that the local environment of each surface-attached molecule displays substantial inhomogeneous broadening, most clearly reflected in the distribution of peak potentials and widths of the Gaussian derivative correlations at different parts of the surface. Such broadening is interesting and perhaps not unexpected as the potential scans in principle follow individual molecules and not statistical assemblies as when electrochemical ET or ET in homogeneous solution is addressed.

5.3. A Submolecular Feature in the in Situ STM Images of the Blue Single-Copper ET Protein Azurin Adsorbed on Au(111). The azurins belong to the class of blue single-copper ET proteins.[63,64] High-resolution three-dimensional structures[65] and a wealth of physical chemical properties of wild-type and mutant azurins are available. The following is of importance in the present discussion.

(a) The molecule is oblong, ellipsoid-like, with the Cu atom located toward one "end" of the molecule.

(b) A disulfide group is located in the surface of the molecule, at the end opposite to the Cu atom and suitable for gentle linking of the molecule to surfaces of gold and other electronically soft metals.

(c) Facile long-range ET *through* the protein can occur such as shown by studies of intramolecular ET from the disulfide radical anion prepared by pulse radiolysis, to the oxidized Cu center.[66]

(d) Reversible, promoter-free cyclic voltammetry of azurin on pyrolytic graphite is straightforward.[67] Reversible voltammetry of azurin on gold is also feasible but the signal decays within ≈15 min as adsorbed monolayer formation through the disulfide group progresses.[67]

Adsorbed azurin on Au(111) has been investigated to molecular resolution by in situ STM and AFM.[33] In situ STM images are reproducible over almost 0.5 V across the standard

reduction potential. Submolecular resolution shows, moreover, consistently a small central area (i.e., significantly smaller than the total molecular cross section) with an apparent height two to four times larger than closer to the molecular periphery.[33,68] This is in line with the tunnel enhancement by the local redox level of the copper atom and with Tao's observation. Investigations of current−voltage relations are in progress.

6. Concluding Remarks

The formalism in previous sections holds particularly two perspectives. It addresses, first, tunneling in large transition metal complexes and redox metalloproteins in a new way. Emphasis has been on the (strong) electronic-vibrational coupling feature while the electronic interaction between the metallic electrodes and the molecular redox level has been crudely represented, by the Gamov tunneling factor referring to individual electronic levels in the substrate and tip. This limitation can be relaxed and more sophisticated representations introduced, in principle, straightforwardly. Such representations could rest on Newns-Anderson theory of adsorption[69] for solute adsorbates,[70] electron density functionals,[43] and Kohn−Sham schemes.[71]

The second perspective is that in situ STM of large redox adsorbates, framed by formalism such as the one in the present report, may hold a clue to the distinction between different tunnel mechanisms. This relates particularly to the distinction between, on one hand, coherent or resonance tunneling activated by multiphonon electronic-vibrational interactions and, on the other hand, sequential two-step ET modes between fully equilibrated electronic-vibrational states. The clue to such a distinction rests on the option specific to in situ STM, in contrast to ex situ STM, that not merely the bias voltage but also the overvoltage can be controlled. The current−overvoltage patterns, with characteristic spectroscopic features (peaks), are thus distinctive for the coherent or resonance modes. Distinction between coherent two-step ET, as described in the previous sections, and a strict three-level resonance mode[26,27] would be hard and ultimately perhaps have to rest on *detection* of the intermediate, temporarily populated redox level in the coherent two-step mode of Figures 1 and 2. Both the coherent two-step and resonance modes are, however, distinguishable from the sequential, equilibrated two-step in situ STM mechanism for which the current−voltage relations reach a pleateau at high overvoltages. In this way in situ STM holds in principle a new approach to this otherwise elusive distinction.

Relations to other three-level processes, particularly resonance Raman spectral and excitation profiles, have also been discussed.[30] Data which illuminate these features have been reported.[21−23,68] These are presently few in number, but further experimental research may warrant more detail in both electronic-vibrational coupling patterns and the potential distribution in the tunnel gap region. A final note of observation in the present investigation is that, when it comes to molecular scale distances, the current−distance relations are controlled approximately equally by the *electronic* tunnel factor and the *nuclear* environmental reorganization. Straightforward reasons for this were given above, and this observation needs attention in future detailed data analysis.

Acknowledgment. Financial support from the EU program INTAS, the Danish Natural Science and Technical Science Research Councils, the Carlsberg, Lundbeck, and Novo Nordisk Foundations, and the Russian Foundation for Basic Research (Grant No. 97-03-32010a) is acknowledged.

Appendix

Derivation of Equation 6. The solvent reorganization Gibbs free energy is, generally[45,49,56]

$$E_R = \frac{1}{8\pi}\int_V \vec{D}^2 \, dV \tag{A1}$$

where $\vec{D}$ is the vacuum electric field (induction). The volume of integration is the whole space between the substrate and tip, outside the adsorbate molecule. $\vec{D}$ is determined by the electrostatic potential in the dielectric medium, φ_{diel}[57]

$$\vec{D} = \epsilon_s \nabla\vec{\varphi}_{diel} \tag{A2}$$

and related to the vacuum potential, φ_{vac}, by

$$\varphi_{diel} = \epsilon_s^{-1}\varphi_{vac} \text{ or } \vec{D} = -\nabla\vec{\varphi}_{vac} \tag{A3}$$

giving

$$E_R = \frac{1}{8\pi}(\epsilon_o^{-1} - \epsilon_s^{-1})\int_V \nabla\vec{\varphi}_{vac}\nabla\vec{\varphi}_{vac} \, dV \tag{A4}$$

Equation A3 can be converted to surface integral form. Since, further $\varphi_{vac} = 0$ at the metallic surfaces, only the molecular surface, S_a contributes, i.e.

$$E_R = \frac{1}{8\pi}(\epsilon_o^{-1} - \epsilon_s^{-1})\int_{S_a} \nabla\vec{\varphi}_{vac}\nabla\vec{\varphi}_{vac} \, dS_a \tag{A5}$$

Calculation of E_R by eq A5 thus involves construction of the potential φ_{vac} followed by calculation of the surface integral. We consider these two stages separately.

Electrostatic Potential in Image Charge Representation. We shall derive φ_{vac} by the method of image charges.[57,58] φ_{vac} is recast as a superposition of the Coulombic potentials of a point charge e at the adsorbate center, and two infinite sums of potentials of image point charges inside the substrate and tip electrodes. The image charges are denoted as em_n and et_n, and their positions from the electrode−solution interfaces as d_n and l_n, respectively ($n = 1, 2, ..., \infty$) (Figure 3). The charges and distances are derived by the following reasoning. We first insert an image charge of $em_1 = -e$ at $d_1 = -d$ inside the substrate metal, symmetrically opposite to the adsorbate center. The electrostatic potential at the point $\vec{r}$ in the solution is then

$$\varphi_{m1} = \frac{e}{|\vec{r}|} + \frac{em_1}{|\vec{r} + \vec{d} + \vec{d}_1|} \tag{A6}$$

and must accord with the condition $\varphi_{vac}|_{int} = 0$ at the interface. This condition is not, however, satisfied at the tip−solution interface. The first tip image charge et_1 is therefore inserted at the point l_1, symmetrically opposite the real adsorbate charge with respect to the tangential tip plane parallel to the substrate surface. et_1 and l_1 must follow the relations

$$(l + R)(R - l_1) = R^2,\ l_1 = Rl/(R + l)$$

$$\frac{e}{l} = \frac{et_1}{l_1} \tag{A7}$$

The potential

$$\varphi_{t1} = \frac{e}{|\vec{r}|} + \frac{et_1}{|\vec{r} + \vec{l} + \vec{l}_1|} \tag{A8}$$

then also accords with $\varphi_{t1}|_{\text{int}} = 0$ at the tip interface. The potentials of the images therefore compensate the real potential from the molecular center separately at the substrate−solution and solution−tip interface.

The first two image charges do not, however, compensate the real charge potential at *both* interfaces. In a second step, a new pair of image charges em_2 and et_2 is therefore introduced. For the substrate surface

$$em_2 = -et_1;\ d_2 = d + l + l_1 \tag{A9}$$

in the potential form

$$\varphi_{m2,t1} = \frac{e}{|\vec{r}|} + \frac{em_1}{|\vec{r} + \vec{d} - \vec{d}_1|} + \frac{et_1}{|\vec{r} + \vec{l} - \vec{l}_1|} + \frac{em_2}{|\vec{r} + \vec{d} - \vec{d}_2|} \tag{A10}$$

The conditions

$$(R + l + d + d_1)(r - l_2) = R^2 \text{ or } l_2 = \frac{R(l + d + d_1)}{R + l + d + d_1}$$

$$\frac{em_1}{d_1 + d + l} = -\frac{et_2}{l_2} \tag{A11}$$

now ensure that the potential

$$\varphi_{m1,t2} = \frac{e}{|\vec{r}|} + \frac{em_1}{|\vec{r} + \vec{d} + \vec{d}_1|} + \frac{et_1}{|\vec{r} + \vec{l} - \vec{l}_1|} + \frac{et_2}{|\vec{r} + \vec{l} - \vec{l}_2|} \tag{A12}$$

accords with $\varphi_{m1,t2}|_{\text{int}} = 0$ at the tip interface. By including all successive steps in this procedure the overall vacuum potential is

$$\varphi_{\text{vac}} = \frac{e}{|\vec{r}|} + \sum_{n=1}^{\infty} \frac{em_n}{|\vec{r} + \vec{d} - \vec{d}_n|} + \sum_{k=1}^{\infty} \frac{et_k}{|\vec{r} + \vec{l} - \vec{l}_n|} \tag{A13}$$

This potential accords with $\varphi_{\text{vac}}|_{\text{int}} = 0$ at both interfaces simultaneously.

Equation A13 can be given another palatable form. We introduce the short-hand notation

$$em_0 \equiv e;\ d_0 = -d;\ et_0 \equiv e;\ l_0 = l \tag{A14}$$

The following recurrency equations then determine the image charges and their positions

$$em_n = -et_{n-1};\ d_n = d + l + l_{n-1}$$

$$l_n = \frac{R(d + l + d_{n-1})}{R(d + l + d_{n-1})}$$

$$et_n = -\frac{em_{n-1} l_n}{l + d + d_{n-1}};\ n \geq 1 \tag{A15}$$

Another convenient set can be obtained by substituting l_n into d_n

$$d_{n+2} = d + l + \frac{R(d + l + d_n)}{R + d + l + d_n}$$

$$em_{m+2} = em_n \frac{R}{R + d + l + d_n} \tag{A16}$$

and

$$l_{n+2} = \frac{R(2d + 2l + l_n)}{R + 2d + 2l + l_n}$$

$$et_{n+2} = et_n \frac{R}{R + 2d + 2l + l_n} \tag{A17}$$

Taking separately "initial" values for odd and even members of the series, then

$$\text{For } n = 0\text{: } d_o = -d;\ em_0 = e;\ l_0 = -l;\ et_0 = e$$

$$\text{For } n = 1\text{: } d_1 = d;\ et_1 = -e\frac{R}{R + l};\ l_1 = \frac{Rl}{R + l};\ em_1 = -e \tag{A18}$$

All the values and positions of the image charges in eq A13 can therefore be obtained straightforwardly from eqs A16 and A17 and the "initial" values in eq A18.

Solvent Reorganization Gibbs Free Energy in the Image Charge Representation. We now combine eq A5 with the image charge representation in eq A13

$$E_{\text{R}} = \frac{1}{8\pi}(\epsilon_{\text{o}}^{-1} - \epsilon_{\text{s}}^{-1}) \int \text{d}\vec{S}_a \left[\frac{e}{\vec{r}} + \sum_{n=1}^{\infty} \left(\frac{em_n}{|\vec{r} + \vec{d} - \vec{d}_n|} + \frac{et_n}{|\vec{r} + \vec{l} - \vec{l}_n|} \right) \right] \text{grad} \left[\frac{e}{|\vec{r}|} + \sum_{k=1}^{\infty} \left(\frac{em_k}{|\vec{r} + \vec{d} - \vec{d}_k|} + \frac{et_k}{|\vec{r} + \vec{l} - \vec{l}_k|} \right) \right] \tag{A19}$$

From previous investigations[59,60]

$$\int \text{d}\vec{S}_a \frac{e}{|\vec{r}|} \vec{\nabla} \frac{e}{|\vec{r}|} = \frac{4\pi a^2}{a^3} e^2;\ \int \text{d}\vec{S}_a \frac{e}{|\vec{r}|} \vec{\nabla} \frac{em_k}{|\vec{r} + \vec{d} - \vec{d}_k|} = 0 \quad \text{(for any } k\text{)}$$

$$\int \text{d}\vec{S}_a \frac{e}{|\vec{r}|} \vec{\nabla} \frac{et_k}{|\vec{r} + \vec{l} - \vec{l}_k|} = 0$$

$$\int \text{d}\vec{S}_a \frac{em_n}{|\vec{r} + \vec{d} - \vec{d}_n|} \vec{\nabla} \frac{e}{|\vec{r}|} = \frac{4\pi e(em_n)}{d + d_n}$$

$$\int \text{d}\vec{S}_a \frac{et_n}{|\vec{r} + \vec{l} - \vec{l}_n|} \vec{\nabla} \frac{e}{|r|} = \frac{4\pi e(et_n)}{l + l_n} \tag{20}$$

($\vec{d}$ and $\vec{d}_n$ are directed oppositely; so are $\vec{l}$ and $\vec{l}_n$). Terms where the integrand contains combinations of potentials and gradient potentials solely from the image charges can also be included. They will be neglected as they are of the order a^3/R^4 and

commonly taken as the "cutting off effect"[60] Altogether, then, eq 6 emerges.

References and Notes

(1) *Metal Ions in Biological Systems;* Sigel, H., Sigel, A., Eds.; Dekker: New York, 1991; Vol. 27.

(2) Winkler, J. R.; Gray, H. B. *Chem. Rev.* **1992**, *92*, 399−404.

(3) Bixon, M.; Jortner, J.; Michel-Beyerle, M. E. *Biochim. Biophys. Acta* **1991**, *1056*, 301−315, and references therein.

(4) *Chem. Phys*. **1993**, *176*, 289−649; Meyer, T. J., Newton, M. D., Eds.; special issue on electron transfer.

(5) Moser, C. C.; Keske, J. M.; Warncke, K. Farid, R. S.; Dutton, P. L. *Nature* **1992**, *355*, 796−802.

(6) Christensen, H. E. M.; Conrad, L. S.; Mikkelsen, K. V.; Nielsen, M. K.; Ulstrup, J. *Inorg. Chem.* **1990**, *29*, 2808−2816.

(7) Onuchic, J. N.; Beratan, D. N. *J. Chem. Phys*. **1990**, *92*, 722−733.

(8) Skourtis, S.; Beratan, D. N. J. Biol. *Inorg. Chem*. **1997**, *2*, 378−386.

(9) Gruschus, J. M.; Kuki, A. *J. Phys. Chem*. 1**993**, *97*, 5581−5593.

(10) Stuchebrukhov, A. A.; Marcus, R. A. *J. Phys. Chem.* **1995**, *99*, 7581−7590.

(11) Iversen, G.; Kharkats, Yu. I.; Kuznetsov, A. M.; Ulstrup, J. *Adv. Chem. Phys*., in press.

(12) For a list of many systems, see: Canters, G. W.; Dennison, C. *Biochimie* **1995**, *77*, 506−515.

(13) *Protein Electron Transfer*; Bendall, D. S., Ed.; BIOS: Oxford, 1996.

(14) *Adv. Chem. Phys.* **1998**; Bixon, M.; Jortner, J., Eds.; special volumes on electron transfer. In press.

(15) Siddarth, P.; Marcus, R. A. *J. Phys. Chem*. **1993**, 97, 2400−2405, and references there.

(16) Hu, Y.; Mukamel, S. *J. Chem. Phys*. **1989**, *91*, 6973−6988.

(17) Andersen, J. E. T.; Møller, P.; Pedersen, M. V.; Ulstrup, J. *Surf. Sci*. **1995**, *325*, 193−205.

(18) Zhang, J.; Chi, Q.; Dong, S.; Wang, E. *Bioelectrochem. Bioeng*. **1996**, *39*, 267−274.

(19) Zhang, B.; Wang, E. *Probe Micros*. **1997**, *1*, 57−64.

(20) Andersen, J. E. T.; Olesen, K. G.; Danilov, A. I.; Foverskov, C. E.; Møller, P.; Ulstrup, J. *Bioelectrochem. Bioeng*. **1997**, *44*, 57−63.

(21) Tao, N. J. *Phys. Rev. Lett.* **1996**, *76*, 4066−4069.

(22) Han, W.; Durantini, E. N.; Moore, T. A.; Moore, A. L.; Gust, D.; Rex, P.; Leatherman, G.; Seely, G. R.; Tao, N.; Lindsay, S. M. *J. Phys. Chem.* **1997**, *101*, 10719−10725.

(23) Friis, E. P.; Andersen, J. E. T.; Madsen, L. L.; Møller, P.; Ulstrup, J. *J. Electroanal. Chem*. **1997**, *431*, 35−38.

(24) Danilov, A. I. *Russ. Chem. Rev.* **1995**, *64*, 767−781.

(25) Deleted in proof.

(26) Schmickler, W.; Widrig, C. *J. Electroanal. Chem*. **1992**, *336*, 213−221.

(27) Schmickler, W. *Surf. Sci*. **1995**, *295*, 43−56.

(28) (a) Kuznetsov, A. M.; Ulstrup, J. *Chem. Phys*. **1991**, *157*, 25−33. (b) Kuznetsov, A. M.; Ulstrup, J. *Surf. Coat. Technol*. **1994**, *67*, 193−200.

(29) Kuznetsov, A. M.; Sommer-Larsen, P.; Ulstrup, J. *Surf. Sci.* **1992**, *275*, 52−64.

(30) Andersen, J. E. T.; Kornyshev, A. A.; Kuznetsov, A. M.; Madsen, L. L.; Møller, P.; Ulstrup, J. *Electrochim. Acta* **1997**, *42*, 819−831.

(31) For an overview, see: Kharkats, Yu. I.; Kuznetsov, A. M.; Ulstrup, J. *J. Phys. Chem*. **1995**, *99*, 13545−13554.

(32) German, E. D.; Kuznetsov, A. M. *Electrochim. Acta* **1981**, *26*, 1595−1608.

(33) Friis, E. P.; Andersen, J. E. T.; Møller, P.; Nichols, R. J.; Ulstrup, J. *Electrochim. Acta* **1998**, *43*, 2883−2897.

(34) Vol'kensthtein, M. V.; Dogonadze, R. R.; Madumarov, A. K.; Kharkats, Yu. I. *Dokl. Akad. Nauk SSSR, Ser. Fiz.* **1971**, *199*, 124−127.

(35) Dogonadze, R. R.; Ulstrup, J.; Kharkats, Yu. I. *J. Electroanal. Chem.* **1972**, *39*, 47−61.

(36) Kharkats, Yu. I.; Madumarov, A. K.; Vorotyntsev, M. A. *J. Chem. Soc., Faraday Trans. 2* **1974**, *70*, 1578−1590.

(37) Kuznetsov, A. M.; Kharkats, Yu. I. *Elektrokhimiya* **1976**, *12*, 1277−1283.

(38) *Femtosecond Chemistry*; Manz, J.; Wöste, L., Eds.; Verlag Chemie: Weinheim, 1995.

(39) *Femtochemistry. Ultrafast Chemical and Physical Processes in Molecular Systems*; Chergui, M., Ed.; World Scientific: Singapore, 1996.

(40) Zhu, L.; Sage, J. T.; Champion, P. M. *Science* **1994**, *234*, 629−632.

(41) Stock, G.; Domcke, W. *J. Phys. Chem*. **1993**, *97*, 12466−12472.

(42) Seidner, L.; Stock, G.; Domcke, W. *J. Chem. Phys.* **1995**, *103*, 3998−4011.

(43) Kornyshev, A. A.; Kuznetsov, A. M.; Ulstrup, J. *J. Phys. Chem.* **1994**, *98*, 3832−3837.

(44) Kharkats, Yu. I.; Kuznetsov, A. M.; Ulstrup, J. in preparation.

(45) (a) Marcus, R. A. *J. Chem. Phys.* **1956**, *24*, 966−978. (b) Marcus, R. A. *J. Chem. Phys.* **1965**, *43*, 679−701.

(46) Levich, V. G.; Dogonadze, R. R. *Dokl. Akad. Nauk SSSR, Ser. Fiz. Khim*. **1959**, *124*, 123.

(47) Dogonadze, R. R. *Reactions of Molecules at Electrodes*; Hush, N. S., Ed.; Wiley: London, 1971; pp 135−227.

(48) Dogonadze, R. R.; Kuznetsov, A. M. *Prog. Surf. Sci.* **1975**, *6*, 1−42.

(49) Kuznetsov, A. M. *Charge Transfer in Physics, Chemistry, and Biology*; Gordon & Breach: Reading, 1995; p 126.

(50) (a) Marcus, R. A., *Can. J. Chem* **1959**, *37*, 155−162. (b) Hush, N. S. *Trans. Faraday Soc*. **1961**, *57*, 557−580.

(51) Gerischer, H. *Z. Phys. Chem.* **1960**, *26*, (a) 223−247; (b) 325−338.

(52) Dogonadze, R. R.; Chizmadzhev, Yu. A. *Dokl. Akad. Nauk SSSR, Ser. Fiz. Khim.* **1962**, *144*, 1077−1080.

(53) Contributions in: *Tunneling in Biological Systems*; Chance, B., DeVault, D. C., Frauenfelder, H., Marcus, R. A., Schrieffer, J. R., Sutin, N., Eds.; Academic Press: New York, 1979.

(54) Krishtalik, L. I.; Kharkats, Yu. I. *J. Theor. Biol.* **1985**, *112*, 221−249.

(55) Kharkats, Yu. I.; Ulstrup, J. *Chem. Phys.* **1991**, *141*, 117−129.

(56) Pekar, S. I. *Untersuchungen über die Elektronentheorie der Kristalle*; Akademie Verlag: Berlin, 1954.

(57) Landau, L. D.; Lifshitz, E. M. *Electrodynamics of Continuous Media*; Pergamon: Oxford, 1960.

(58) Stratton, J. A. *Electromagnetic Theory*; McGraw-Hill: New York, 1941.

(59) Kharkats, Yu. I. *Elektrokhimiya* **1976**, *12*, 592−595.

(60) Kharkats, Yu. I. *Elektrokhimiya* **1978**, *14*, 1721−1724.

(61) Mazur, U.; Hipps, K. W. *J. Phys. Chem.* **1995**, *99*, 6684−6688.

(62) Lu, X.; Hipps, K. W. *J. Phys. Chem.* **1997**, *101*, 5391−5496.

(63) Sykes, A. G. *Adv. Inorg. Chem.* **1991**, *36*, 377−408.

(64) Farver, O. *Protein Electron Transfer*; Bendall, D. S., Ed.; BIOS: Oxford, 1996; pp 161−188.

(65) Nar, H.; Messerschmidt, A.; Huber, R. *J. Mol. Biol*. **1991**, *221*, 765−772.

(66) Farver, O.; Skov, L. K.; Pascher, T.; Karlsson, B. G.; Nordling, M.; Lundberg, L. G.; Vänngård, T.; Pecht, I. *Biochemistry* **1993**, *32*, 7317−7322.

(67) Friis, E. P.; Andersen, J. E. T.; Madsen, L. L.; Bonander, N.; Møller, P.; Ulstrup, J. *Electrochim. Acta* **1997**, *42*, 2889−2897. Erratum: *Electrochim. Acta* **1998**, *43*, 1114−1122.

(68) Iversen, G.; Friis, E. P.; Kharkats, Yu. I.; Kuznetsov, A. M.; Ulstrup, J. *J. Biol. Inorg. Chem*. **1998**, *3*, 229−235.

(69) Muscat, J.; Newns, D. N. *Prog. Surf. Sci.* **1978**, *9*, 1−43.

(70) Kuznetsov, A. M.; Ulstrup, J. *J. Electroanal. Chem.* **1985**, *195*, 1−19.

(71) (a) Kornyshev, A. A.; Kuznetsov, A. M.; Makov, G.; Vigdorovich, M. V. *J. Chem. Soc., Faraday Trans.* **1996**, *92*, 3997−4004. (b) **1996**, *92*, 4005−4014.